let station

$\bar{\mathbf{p}}$ = fractional input matrix augmented to include an accumulating station

$g_{ij}$ = volumetric flow rate from region $i$ to region $j$

$g'_{ij}$ = volumetric flow rate from region $i$ to region $j$ for stirred-tank network model

$r_{ij}$ = fractional input coefficient from tank $i$ to tank $j$ for stirred-tank network, see Equation (34) for special definition of $r_{jj}$

$\mathbf{R}$ = matrix of fractional input coefficients for the stirred-tank network model

$\mathbf{R}_{\text{In}}$ = matrix of fractional input coefficients from the inlet station top the stirred-tank network model

$s_{ij}$ = steady response at region $j$ to a steady tracer input into region $i$

$\mathbf{S}$ = matrix of steady response coefficients

$t$ = time

$V_i$ = volume of the $i^{\text{th}}$ region

$V_i'$ = volume of the $i^{\text{th}}$ tank in the stirred-tank network model

$\mathbf{V}$ = volume column vector

$\mathbf{V}'$ = volume column vector for the stirred tank network model

$\alpha_i$ = coefficients in the Caley-Hamilton equation

$\lambda$ = eigenvalue

$\Delta t$ = single transition time interval

## LITERATURE CITED


Buffham, B. A., L. G. Gibilaro, and H. W. Kropholler, "Network Combing of Complex Flow-Mixing Models," *Chem. Eng. Sci.*, 24, 7 (1969).

Rubinow, S. I., "Some Mathematical Problems in Biology," *Bull. Am. Math. Soc.*, 81, 782 (1975).

Wen, C. T., and L. T. Fan, *Models for Flow Systems and Chemical Reactors*, McGraw-Hill, New York (1975).



*Manuscript received July 12, 1976; revision received May 2 and accepted May 12, 1977.*


# The Permeation of Gases Through Hollow Silicone Rubber Fibers: Effect of Fiber Elasticity on Gas Permeability


**S. A. STERN**
**F. J. ONORATO**
**and**
**CHARLES LIBOVE**

**Department of Chemical Engineering and Materials Science**
**Syracuse University**
**Syracuse, New York 13210**



The permeation of oxygen, nitrogen, argon, and synthetic air through hollow silicon rubber fibers was studied between 0° and 40°C and at gauge pressures of up to $3.45 \times 10^5$ N/m$^2$ (50 lb/in.$^2$ abs). The study was conducted in a permeator module in which the hollow fibers were pressurized externally. Strain measurements with single fibers showed this mode of operation to be preferable to internal pressurization. The gas permeation rates were markedly affected by dimensional changes of the hollow fibers under external pressure. These changes were predicted satisfactorily by a modification of Varga's (1966) deformation analysis of thick-walled elastic tubes. The extent of air separation achieved in the permeator was in agreement with that calculated from theoretical models. It is conjectured that the performance of such a permeator may be improved in certain cases if the fibers are under suitable initial tension.


## SCOPE

The development of hollow fiber permeators has been one of the most important advances in membrane separation technology in recent years. Such permeators, which use hollow polymer fibers as separation barriers, offer important advantages over permeator modules employing spiral or flat sheet membranes. One advantage is that a much larger membrane area can be packed per unit permeator volume, thus greatly reducing capital investment costs. Another advantage is that hollow fiber permeators do not require costly membrane supports and are more damage-resistant than other types of permeators. Hollow fiber permeators are being used on a large scale for water desalination and purification and are also being considered for the separation of various gas mixtures.

Silicone rubber is a membrane material of particular interest for gas separations because it exhibits a very high gas permeability compared to other polymers. For example, silicone rubber membranes, either in hollow fiber or sheet form, have been employed for biomedical applications and are potentially useful for the inerting of fuel tanks of jet transports and in the nuclear industry.


C. Libove is at the Department of Mechanical and Aerospace Engineering, Syracuse University.

Correspondence concerning this paper should be addressed to S. A. Stern.

Very few studies have been reported in the literature on the permeation of gases through hollow silicone rubber fibers, and consequently a number of important questions remain to be answered. Thus, in the construction of permeators with bundles of such fibers, it is important to know whether it is more advantageous to pressurize the fibers internally or externally. Only the former mode of operation was investigated in previous studies. In either case, the fibers will undergo significant dimensional changes which will affect both gas permeation rates and the pressure drop inside and outside the fibers. These dimensional changes will also affect the fiber packing density in the permeator. The objective of the present work was to examine some of these problems and to provide criteria for the construction of efficient gas permeators with hollow elastic fibers.

## CONCLUSIONS AND SIGNIFICANCE

The present work indicates that it is possible to build efficient permeator modules with hollow silicone rubber fibers which can operate at elevated pressures. Such modules can be utilized for the separation of gases in single or multistage processes. The high-pressure gas stream in such permeators should flow preferably outside the hollow fibers, at least in the case of the fibers used in the present work [$6.35 \times 10^{-4}$ m ($2.5 \times 10^{-2}$ in.) O.D. $\times$ $3.05 \times 10^{-4}$ m ($1.2 \times 10^{-2}$ in.) I.D.]. Externally pressurized fibers undergo two types of elastic deformations: the cross section decreases, causing an increase in the O.D./I.D. ratio, and the length of the fibers increases. The deformations are a function of the pressure difference across the fiber walls and affect the rates of gas permeation through the walls. The magnitude of these effects can be estimated from theoretical considerations.

The separation of gas mixtures in a permeator module, or stage, with hollow silicone rubber fibers can be predicted with confidence from theoretical models, if the components of the mixtures exhibit low solubilities in the fibers. The extent of separation achievable with a particular mixture, such as the synthetic air used in the present study, will depend on the temperature, the pressure inside and outside the hollow fibers, the flow pattern in the stage, and the stage cut. The design of cascades of such permeators should present no difficulties.

---

The selective permeation of gases through nonporous polymeric membranes is being studied in a number of laboratories as a potential technique for the separation of gas mixtures of industrial interest. One of the most important advances in this field in recent years is the development of hollow fiber membranes and of permeation equipment (permeators) employing such membranes. The advantages of hollow fiber permeators, which are already being used on a large scale for water desalination, have been summarized by Mattson and Tomsic (1969):

(a) A very large membrane area can be packed per unit volume of permeator vessel. Thus, an area of about $3.94 \times 10^4$ m$^2$/m$^3$ ($1.20 \times 10^4$ ft$^2$/ft$^3$) has been mentioned by Mattson and Tomsic for small bore fibers with an O.D. of $4.5 \times 10^{-5}$ m ($1.8 \times 10^{-3}$ in). By contrast, membrane areas of only 656 to 984 m$^2$/m$^3$ (200 to 300 ft$^2$/ft$^3$) are obtained in permeators using sheet membranes.

(b) Some types of hollow fibers, such as those made of polyester, have high strength and can support themselves under gauge pressures as high as $7.0 \times 10^6$ N/m$^2$ (1 000 lb/in.$^2$). Therefore, hollow fiber membranes do not require costly, space consuming porous supports as do sheet membranes.

(c) The resistance of inelastic hollow fibers to collapse is dependent on the ratio of the internal to the external diameter, as is the case for heavy walled cylinders. When this ratio is maintained constant, the resistance of the hollow fibers to applied stress does not depend on wall thickness. Hence, it is possible to reduce the wall thickness of the fibers without significant loss in strength.

(d) The wall thickness of some types of hollow fibers can be reduced to less than $1.3 \times 10^{-5}$ m ($5 \times 10^{-4}$ in.), thereby greatly increasing permeation rates and decreasing the required membrane area.

The use of hollow fibers as separation barriers can markedly reduce the unit permeator cost, provided that the cost of the fibers is not a limiting factor. Hollow fibers have been made from a variety of polymers including polyester (dacron), polyamide (nylon), silicone rubber, cellulose ethers, cellulose esters, and polycarbonate. Silicone rubber [poly(dimethyl siloxane)] has the highest permeability to simple gases of all polymers, and consequently its use as a gas separation barrier is of particular interest.

When a hollow fiber permeator is designed for a gas separation process, it is necessary to decide whether the high-pressure feed gas should be allowed to flow inside or outside the hollow fibers. The relative merits of these two modes of operation have not yet been discussed in the literature. This problem is particularly important when the hollow fibers are made from an elastomer, such as silicone rubber, rather than from a rigid polymer. If the gas pressure is applied externally, thin silicone rubber fibers will tend to collapse, probably at lower pressures than comparable rigid fibers. On the other hand, if the gas pressure is applied internally, the silicone rubber fibers will expand and eventually rupture. In either case, the dimensions of the fibers will be a function of pressure.

Theoretical and experimental studies on gas permeation and separation using hollow silicone rubber fibers appear to have been reported only by Blaisdell and Kammermeyer (1972, 1973) and by Thorman, Rhim, and Hwang (1975). In all these studies the hollow fibers were pressurized internally. Blaisdell and Kammermeyer (1973) have investigated the permeation of oxygen through several sizes of silicone rubber fibers as a

function of the pressure difference across the fiber wall. The smallest hollow fibers had an O.D. of $3.81 \times 10^{-4}$ m ($1.5 \times 10^{-2}$ in.) and an I.D. of $2.54 \times 10^{-4}$ m ($1.0 \times 10^{-2}$ in.), while the corresponding dimensions of the largest fibers were $1.96 \times 10^{-3}$ m ($7.7 \times 10^{-2}$ in.) and $1.47 \times 10^{-3}$ m ($5.8 \times 10^{-2}$ in.). The changes in the radial dimensions of the fibers due to applied internal pressure could be predicted by means of a relation derived from linear elasticity. However, this relation was found to hold only when the fractional change in diameter was small (<0.2). The pressure drop across the fiber walls in these studies was less than $1.86 \times 10^5$ N/m² (27 lb/in.²). The permeation of gas mixtures has been also studied by Blaisdell and Kammermeyer (1972, 1973) as well as by Thorman, Rhim, and Hwang (1975), but the analysis of their data did not require corrections for dimensional changes in the fibers.

The present paper summarizes the results of a study on the permeation of oxygen, nitrogen, argon, and synthetic air through hollow silicone rubber fibers over a wider range of pressures and temperatures than investigated heretofore. In this work, the hollow fibers were pressurized externally. The paper also presents the results of a theoretical study on the effect of elastic deformations of the hollow fibers, due to applied external pressure, on gas permeability. The theoretical analysis is then compared with the experimental results and practical applications of these results are suggested.

## EFFECT OF FIBER ELASTICITY ON GAS PERMEABILITY

### Formulas for Permeation Rates

The steady-state rate of permeation $G$ of a pure gas through the wall of a homogeneous and isotropic cylindrical tube, when the gas pressures $p_O$ and $p_I$ are maintained at the outer and inner surfaces, respectively, is given by (Stern, 1972*b*):

$$G = \bar{P}\frac{2\pi L(p_O - p_I)}{\ln(R_O/R_I)} \tag{1}$$

$\bar{P}$ depends on the temperature and the pressures $p_O$ and $p_I$. The above equation has been found to be applicable to nonporous cylindrical tubes and hollow fibers made from a variety of synthetic and natural polymers.

Equation (1) applies to an elastic tube as well as to a rigid tube, provided that $L$, $R_O$, and $R_I$ are interpreted as the actual dimensions, taking into account the deformations due to gas pressure, and that the homogeneity of the material in regard to the permeability coefficient $\bar{P}$ is not destroyed by the inhomogeneity of the elastic strains. It will be assumed in what follows that the second proviso is met and, furthermore, that the value of $\bar{P}$ of the strained material is the same as that of the unstrained material. This assumption is justified by the work of Yasuda, Stannett, Frisch, and Peterlin (1964) as well as by the good agreement obtained between the results of the analysis and the experimental data.

Equation (1) may be written with the initial dimensions of the tube appearing in the right-hand side, provided that a correction factor $f_1$ is also included to compensate for the use of the incorrect dimensions. In this way the following alternate formula for $G$ is obtained:

$$G = \bar{P}f_1\frac{2\pi l(p_O - p_I)}{\ln(r_O/r_I)} \tag{2}$$

where $l$, $r_O$, and $r_I$ are the length, outer radius, and inner radius, respectively, of the tube or hollow fiber prior to the application of the pressures $p_O$ and $p_I$, that is, in an ambiance of $1 \times 10^5$ N/m² (14.7 lb/in.² abs) of hydrostatic pressure. Equating the above two expressions for $G$, we get the following formula for the correction factor $f_1$:

$$f_1 = \frac{L}{l}\frac{\ln(r_O/r_I)}{\ln(R_O/R_I)} \tag{3}$$

Still another form of Equation (1) is obtained by combining all the right-side terms of Equation (2), except $\bar{P}$, $l$, and $p_O - p_I$, into a single dimensionless factor $f_2$. The relation thus obtained is

$$G = \bar{P}l(p_O - p_I)f_2 \tag{4}$$

where

$$f_2 = \frac{2\pi f_1}{\ln(r_O/r_I)} = \frac{L}{l}\frac{2\pi}{\ln(R_O/R_I)} \tag{5}$$

In the case of a rigid tube, $f_1$ becomes 1, and $f_2$ reduces to $2\pi/\ln(r_O/r_I)$.

### Theoretical Evaluation of $f_1$ and $f_2$

Either of Equations (2) and (4) can be used to compute the rate of permeation $G$, provided that $f_1$ and $f_2$ are known. The values of these dimensionless factors depend upon the elastic properties of the tube, its initial geometry, and the magnitude of the external and internal pressures. To determine $f_1$ and $f_2$ analytically requires an elastic analysis of the tube, and, inasmuch as we are dealing with an elastomer, this analysis should be based on finite, rather than infinitesimal, elasticity theory. Such an analysis is carried out in the Appendix for the case in which $p_I$ is $1 \times 10^{-5}$ N/m² (14.7 lb/in.² abs), and the material is incompressible and initially isotropic.

The main results of the analysis are given in Figures 1 and 2 in the form of graphs of $f_1$ and $f_2$ for the case

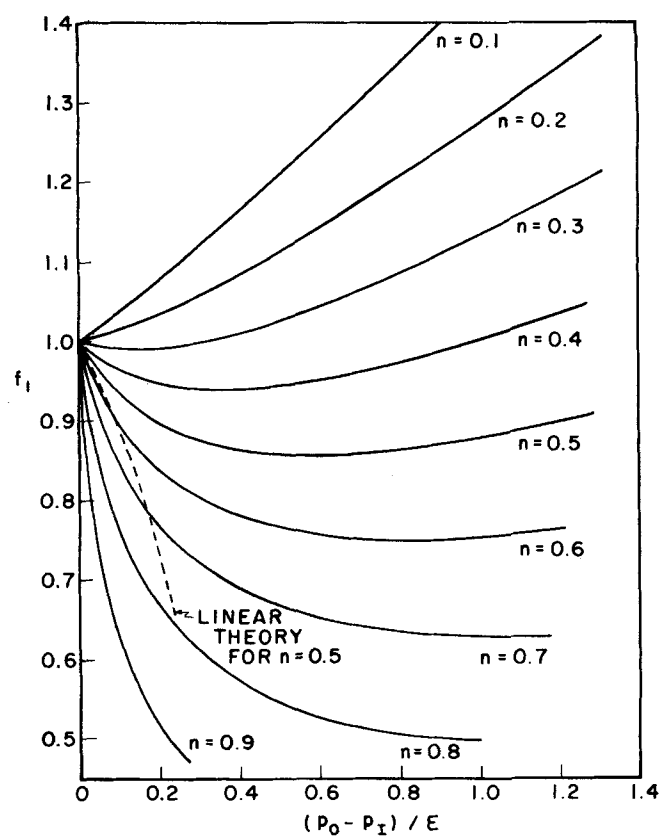


Fig. 1. Graph of correction factor $f_1$ vs. $(p_O - p_I)/E$. Correction factor $f_1$ is defined by Equation (3).

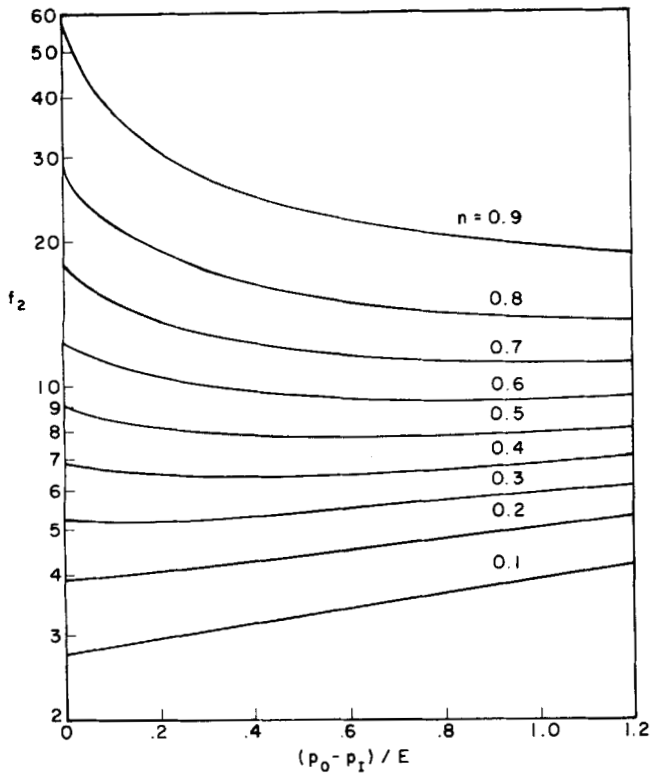


**Fig. 2. Graph of correction factor $f_2$ vs. $(p_O - p_I)/E$. Correction factor $f_2$ is defined by Equation (5).**

$p_O > p_I$. In these figures, $n$ stands for the initial ratio of inner-to-outer radius; that is

$$n \equiv r_I/r_O \tag{6}$$

and $E$ is the Young's modulus of the material, defined, in principle, by the initial slope of the stress-strain curve obtained in a uniaxial tension test. The value $n = 0.48$ is of special interest because it is the best estimate of the $r_I/r_O$ ratio of the hollow fibers used in this experimental investigation, as determined by measurement. For this $n$, the relationship between $f_1$ and $(p_O - p_I)/E$ is given in Table 1.

TABLE 1. VALUES OF THE FUNCTION $f_1$ FOR $n = 0.48$

| $(p_O - p_I)/E$ | $f_1$ |
|---|---|
| 0 | 1 |
| 0.05 | 0.9676 |
| 0.10 | 0.9430 |
| 0.15 | 0.9240 |
| 0.20 | 0.9093 |
| 0.25 | 0.8980 |
| 0.30 | 0.8894 |
| 0.35 | 0.8831 |
| 0.40 | 0.8785 |
| 0.45 | 0.8756 |
| 0.50 | 0.8739 |
| 0.55 | 0.8734 |
| 0.60 | 0.8738 |
| 0.65 | 0.8751 |
| 0.70 | 0.8772 |
| 0.75 | 0.8800 |
| 0.80 | 0.8833 |
| 0.85 | 0.8871 |
| 0.90 | 0.8914 |
| 0.95 | 0.8962 |
| 1.00 | 0.9013 |
| 1.05 | 0.9067 |
| 1.10 | 0.9124 |
| 1.15 | 0.9184 |
| 1.20 | 0.9247 |
| 1.25 | 0.9312 |
| 1.30 | 0.9379 |
| 1.35 | 0.9447 |
| 1.40 | 0.9518 |
| 1.45 | 0.9590 |
| 1.50 | 0.9663 |

An examination of Figure 1 shows that, except for the very thick-walled tubes ($n < 0.25$), the initial effect of the tube's elasticity is to reduce the permeation rate to a value below what it would be for a rigid tube; this is due to the fact that at first the external pressure tends to increase the denominator in Equation (1) faster than it increases the dimension $L$ appearing in the numerator. When the external pressure becomes large, however, the increase of $L$ predominates and the curves of $f_1$ and $f_2$ start to turn upward. For the very thick-walled tubes ($n < 0.25$), the lengthening effect predominates from the start, which explains why the curves for the smaller $n$ values have an upward slope over the entire pressure range.

The dashed curve in Figure 1 is based on infinitesimal elasticity theory. Its deviation from the solid curve for the same value of $n$ shows the unsuitability of infinitesimal elasticity theory for computing the elastic deformations once the external pressure exceeds a few percent of $E$.

Of the two figures, 1 and 2, the second is the more suitable one for showing, at the same time, the effect on permeability of elastic deformations and initial geometry, as reflected in the parameter $r_O/r_I$. This is clear from Equations (2) and (4); in the first, $r_O/r_I$ still appears explicitly, while in the second it does not, implying that its entire effect is contained in $f_2$.

## APPARATUS AND EXPERIMENTAL PROCEDURE

### Permeator Design Considerations

The problem as to whether, in a hollow fiber permeator, the fibers should be pressurized internally or externally, that is, whether the high-pressure gas should flow inside or outside the hollow fibers, was elucidated by the following tests. The fibers used had an O.D. of $6.35 \times 10^{-4}$ m ($2.5 \times 10^{-2}$ in) and an I.D. of $3.81 \times 10^{-4}$ m ($1.5 \times 10^{-2}$ in) and are characterized in more detail in a later section.

The stress-strain behavior of hollow fibers which were pressurized internally was studied with a number of single fibers, each about 0.305 m (12 in.) long. One end of the fiber was sealed, and the other end was connected to a nitrogen cylinder. The fiber was first pressurized under water in order to detect the presence of possible pinholes. A fiber which contained such imperfections was rejected. After the water test, the fiber was mounted on a bench, and a microscope with a magnification of 100× was used to observe the radial expansion of the fiber with increasing internal pressure. The external pressure was atmospheric. The experimental results are shown for five different fibers in Figure 3, where the percentage expansion of the outer radius is plotted as a function of the pressure drop across the fiber wall. All fibers ruptured when the pressure difference across the fiber wall was between $2.76 \times 10^5$ and $3.45 \times 10^5$ N/m² (40 and 50 lb/in.²), mainly because of the presence of thin spots in the fiber walls.

The effect of external pressurization on the hollow fibers was studied by means of the permeator and the experimental technique described below. In this study, the pressure on the fibers was varied, while that inside the fibers was maintained near $1 \times 10^5$ N/m² (14.7 lb/in.² abs). The permeator developed a leak when a gauge pressure of $1.38 \times 10^6$ N/m² (200 lb/in.² gauge) was exceeded, probably due to the failure of its tube sheets. However, the construction of permeators operating at much higher pressures appears to be readily feasible.

In view of the fact that the rate of permeation increases with the pressure difference across the fiber wall $\Delta p$,

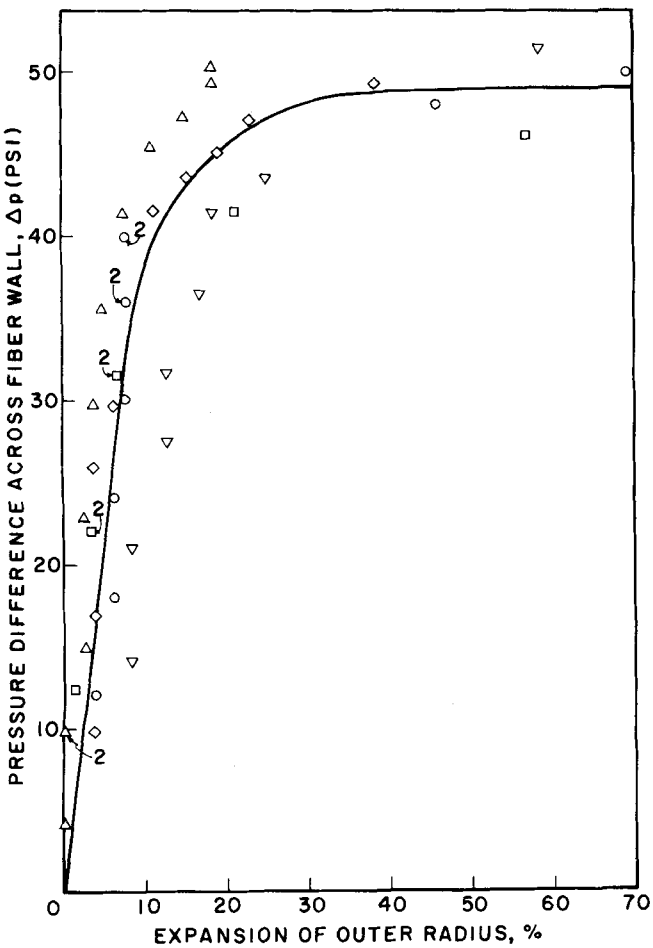


**Fig. 3. Effect of internal pressurization on outer radius of hollow silicone rubber fibers. Dimensions of hollow fibers: 6.35 × $10^{-4}$ m (2.5 × $10^{-3}$ in.) O.D. × 3.05 × $10^{-4}$ m (1.2 × $10^{-2}$ in.) I.D.**

it is desirable to use as large a $\Delta p$ as is compatible with the strength of the fibers, the mechanical integrity of the permeator, and the economics of the separation process under consideration. Since much larger $\Delta p$'s can be used when the fibers are pressurized externally, rather than internally, it appears advantageous to construct and operate a hollow fiber permeator such that the high-pressure gas stream circulates outside the hollow fibers.

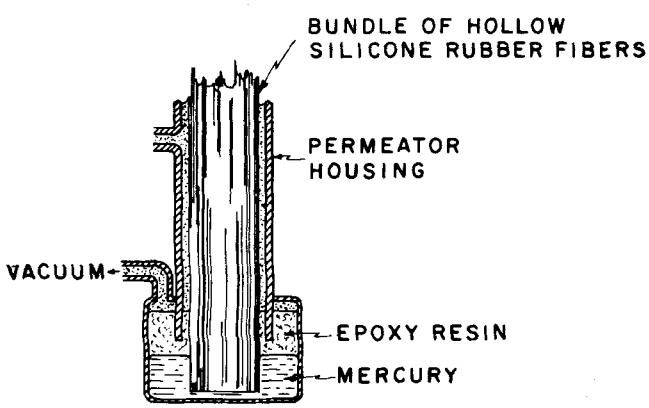


**Fig. 4. Method of casting headers (tube sheets) for bundles of hollow silicone rubber fibers.**

### Construction of a Hollow Fiber Permeator

The permeator was constructed according to a method first described by McAfee (1960), whose pioneering work has not received sufficient recognition. McAfee devised a simple yet reliable technique of forming headers, or tube sheets, for bundles of silica capillaries. This technique can also be applied to hollow polymer fibers and is illustrated in Figure 4. A bundle of such fibers is first inserted inside an appropriate cylindrical high pressure vessel. The vessel is placed in a vertical position, and the lower end of the fiber bundle is immersed in a pool of mercury contained in a closed can. The fibers must be maintained under a slight tension. Epoxy resin and hardener are then mixed and poured on top of the mercury to the desired thickness. The can thus serves as a mold for the fiber tube sheet. The epoxy resin may be outgassed under a mild vacuum. When the epoxy has set, forming a tube sheet, the bundle is removed from the can and the fiber ends are cut to the level of the epoxy seal. The mercury prevents the hollow fibers from being clogged with epoxy during the casting operation. The sealing of the epoxy to the fibers takes place as a result of the strong compressive forces of the epoxy; since most resins contract slightly on setting, the bond is quite strong (McAfee, 1960).

The forming of tube sheets of hollow silicone rubber fibers presents a special problem because these fibers are not wetted by epoxy resin, and consequently the tube sheets are not gas-tight. This problem was solved by casting the tube sheet in the form of a three-layered sandwich which consisted of two outer layers of Armstrong A-271 epoxy adhesive and an inner layer of General Electric RTV-30 silicone rubber sealant. The latter compound provided a gas-tight seal between the epoxy resin and the hollow fibers as well as the internal surface of the pressure vessel. All surfaces exposed to the silicone rubber compound were first cleaned with xylene and pretreated with General Electric SS-4124 silicone plastics primer. Each one of the three layers of the tube sheet was allowed to cure for a minimum of 24 hr. The entire tube sheet was completely cured in a period of 2 wk.

The permeator used in the present study is shown in Figure 5. It was constructed from a section of heavy-walled Plexiglas tubing which was about 0.457 m (18 in.) long and had an O.D. of 6.35 × $10^{-2}$ m (2.5 in.) and an I.D. of 5.08 × $10^{-2}$ m (2.0 in.). This tubing formed the permeator shell and contained a bundle of 104 hollow silicone rubber fibers. The two ends of the fiber bundle were encased in 3.81 × $10^{-2}$ m (1.5 in.)-thick tube sheets cast by the method described above; each of the three layers of the tube sheets was about 1.27 × $10^{-2}$ m (0.5 in.) thick. The length of the fiber bundle exposed to the gas phase was thus approximately 0.381 m (15 in.). The total permeation area was 0.079 $m^2$ (0.85 $ft^2$), and the membrane packing density was 102 $m^2/m^3$ (31 $ft^2/ft^3$). Much larger packing densities, perhaps by a factor of 100, could have been achieved if required. The ends of the Plexiglas tubing were closed by means of two 3.81 × $10^{-2}$ m (1.5 in.)-thick caps from the same material; one cap was dead-ended, while the other one had an outlet in its center for the permeated product stream. The permeator shell was provided with an inlet for the feed stream and an outlet for the unpermeated product stream. The feed inlet and the two product outlets were located at opposite ends of the permeator, as shown

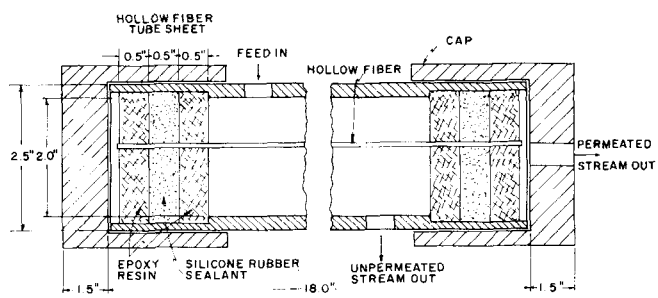


**Fig. 5. Diagram of hollow fiber permeator.**

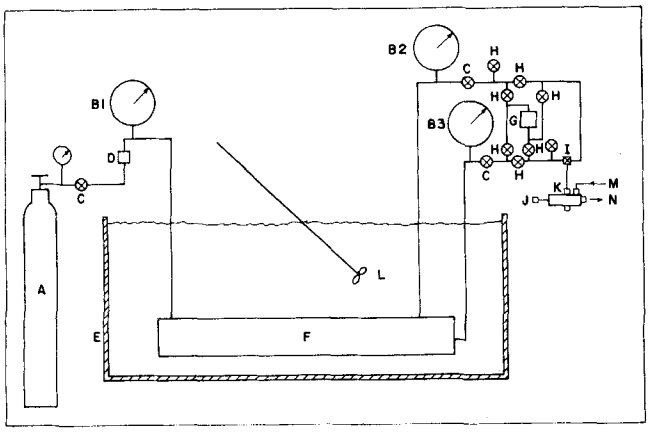


**Fig. 6. Diagram of permeator assembly. $A$ = gas cylinder; $B_1$, $B_2$, $B_3$ = pressure gauges; $C$ = needle valves; $D$ = rotameter; $E$ = constant-temperature bath; $F$ = hollow fiber permeator; $G$ = gas buret for flow rate measurements; $H$ = valves; $I$ = switching valve for gas stream selection; $J$ = actuator for sampling valve; $K$ = sample valve for gas chromatograph; $L$ = stirrer; $M$ = carrier gas, $N$ = sample to gas chromatograph.**

in Figure 5, so as to cause the gas streams inside and outside the hollow fibers to flow cocurrently to one another.

### Permeability Measurements

The rate of permeation of pure gases and gas mixtures through hollow silicone rubber fibers was measured by means of the apparatus shown in Figure 6, which consisted basically of a hollow fiber permeator and a Beckman GC-5 gas chromatograph. With reference to Figure 6, the permeator $F$ was immersed in a thermostatted bath $E$ whose temperature could be maintained constant to within $\pm 0.1$°C in the experimental range from 0° to 40°C. The method used to measure the permeation rate of a pure gas was straightforward. The gas from a cylinder $A$ was admitted to the high-pressure side of the permeator at some convenient pressure $p_O$ which was measured with a 16 in. Heise gauge B1 reading to $3.45 \times 10^3$ N/m$^2$ (0.5 lb/in.$^2$). The outlet on the high-pressure side of the permeator was closed in the tests with pure gases. The permeated gas emerging from the hollow fiber permeator was substantially at atmospheric pressure; that is, $p_I \approx 1 \times 10^5$ N/m$^2$ (14.7 lb/in.$^2$ abs). Its flow rate (the rate of permeation) was measured in a calibrated borosilicate buret $G$ by the water displacement method. Effective permeability coefficients $\bar{P}^e (= \bar{P}f_1)$ for the pure gases were calculated from Equation (1), knowing the permeation rate $G$, the pressures $p_O$ and $p_I$, and using the initial (unstressed) fiber dimensions for $l$, $r_O$, and $r_I$ in place of the current dimensions $L$, $R_O$, and $R_I$.

The permeation of gas mixtures was studied with the same apparatus. The pressure of the feed stream was measured with the Heise gauge mentioned above, and the feed rate was determined with a precision rotameter $D$. The pressure of the unpermeated stream leaving the permeator was measured with a 16 in. Heise gauge B2 reading to $6.9 \times 10^3$ N/m$^2$ (1 lb/in.$^2$). The pressure drop across the high pressure side of the permeator, as determined from gauges B1 and B2, was negligible because of the low flow rate of the high-pressure gas stream. The permeated stream leaving the permeator was at atmospheric pressure, as was ascertained also by means of a 12 in. Heise gauge B3 reading to $1.4 \times 10^3$ N/m$^2$ (0.2 lb/in.$^2$). The flow rates of the permeated and unpermeated streams were measured with water buret $G$. Samples of the two streams were removed by the manipulation of appropriate valves for analysis with the gas chromatograph.

The measurements with pure gases and gas mixtures were conducted over periods of time of at least 5 hr in order to ensure that steady-state conditions had been reached. The gases studied were nitrogen, oxygen, argon, and a mixture of synthetic air.

### Materials

*Hollow Fibers.* The hollow silicone rubber fibers were manufactured by Dow Corning Corporation of Midland, Michigan, and were designed as "Silastic Medical-Grade Tubing." The filler content of the silicone rubber was stated by the manufacturer to be 32.25 ± 3 vol % (51.66 wt %). The density of the polymer was $9.8 \times 10^2$ kg/m$^3$ (61.2 lb/ft$^3$), and that of the silica filler was $2.2 \times 10^3$ kg/m$^3$ (137.3 lb/ft$^3$).

The nominal O.D. and I.D. of the fibers were $6.35 \times 10^{-4}$ m ($2.5 \times 10^{-2}$ in.) and $3.05 \times 10^{-4}$ m ($1.2 \times 10^{-2}$ in.), respectively. The I.D. was determined more accurately from the weight of mercury required to fill a selected length of hollow fiber. A range of I.D. values from $2.7 \times 10^{-4}$ m ($1.07 \times 10^{-2}$ in.) to $3.19 \times 10^{-4}$ m ($1.26 \times 10^{-2}$ in.) was obtained in this manner with eleven fiber samples, the average being $(3.06 \pm 0.149) \times 10^{-4}$ m ($1.20 \times 10^{-2}$ in.). A microscopic observation of the fiber cross section yielded an average I.D. of $(3.020 \pm 0.150) \times 10^{-4}$ m ($1.19 \times 10^{-2}$ in.) and an average O.D. of $(6.426 \pm 0.317) \times 10^{-4}$ m ($2.53 \times 10^{-2}$ in.). These values are based on twenty-four observations. Since the measured inner and outer diameters are very close to their nominal values, the latter were used in all calculations. Hence, the value of the ratio $n (\equiv r_I/r_O)$ was 0.48. The tolerance of fiber wall thickness was stated by the manufacturer to be $\pm 5 \times 10^{-5}$ m ($\pm 2 \times 10^{-3}$ in.).

*Gases.* The pure gases used are listed in Table 2.

Table 2. Gas Purities

| Gas | Grade | Purity, vol % | Suppliers |
|---|---|---|---|
| Nitrogen | High purity | 99.99 min | Union Carbide (Linde) |
| Oxygen | Extra dry | 99.6 min | Union Carbide (Linde) |
| Argon | High purity | 99.996 min | Union Carbide (Linde) |

The gas mixture used was synthetic air supplied by Matheson Gas Products of East Rutherford, New Jersey. The following gas analysis was provided for this mixture by the suppliers:

| | |
|---|---|
| Argon | 0.94 vol % |
| Oxygen | 20.4 vol % |
| Nitrogen | balance |
| Water | < 15 p.p.m. |
| Carbon dioxide | < 10 p.p.m. |
| Total HC | < 1 p.p.m. |

*Epoxy Resin.* Armstrong A-271 Epoxy Adhesive was used as a potting compound because of its high wetting ability, low shrinkage, and low exotherm. This compound was obtained from Armstrong Products Co. of Warsaw, Indiana. Its optimum cure schedules are 30 min at 93°C, or 2 wk at room temperature.

*Sealant and Primer.* RTV-30 sealant is a two-package silicone rubber compound that cures to silicone rubber. Cure time is about 24 hr at room temperature. RTV-30 is pourable. All surfaces exposed to this compound were cleaned with xylene and coated with SS-4125 primer. Both sealant and primer were obtained from General Electric Company, Silicone Products Department, Waterford, New York.

## EXPERIMENTAL RESULTS

### Permeation of Pure Gases

Rates of permeation of nitrogen, oxygen, and argon through hollow silicone rubber fibers were measured at temperatures from 0° to 40°C and at values of the pressure differential $\Delta p (= p_O - p_I)$ of up to $1.38 \times 10^6$ N/m$^2$ (200 lb/in.$^2$). The pressure $p_O$ was varied in these measurements, while $p_I$ was constant at $\sim 1 \times 10^5$ N/m$^2$ (14.7 lb/in.$^2$ abs). The experimental results are

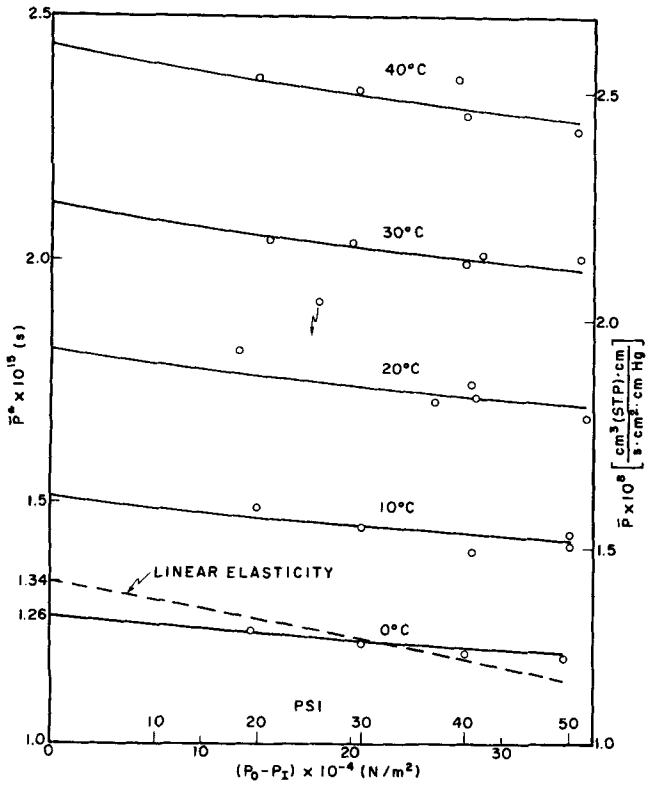


Fig. 7. Effective permeability coefficient for nitrogen as a function of pressure difference across fiber wall.

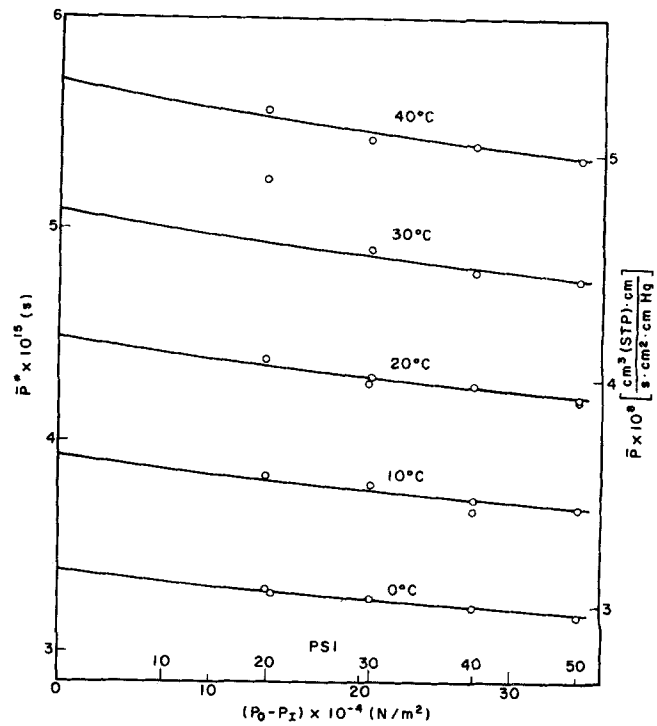


Fig. 8. Effective permeability coefficient for oxygen as a function of pressure difference across fiber wall.

given by the small circles in Figures 7, 8, and 9. These data are in terms of an effective permeability coefficient $\bar{P}^*$, which is the value of $\bar{P}$ computed from Equation (1) when the measured permeation rate is substituted in the left side and the values of $L$, $R_O$, and $R_I$ at $\Delta p = 0$ (that is, the initial values) in the right side, together with the measured $\Delta p$. Thus, $\bar{P}^*$ is defined by the equation

$$G = \bar{P}^* \frac{2\pi l(p_o - p_I)}{\ln(r_O/r_I)} \qquad (7)$$

where $l = 0.381$ m (15 in.) and $r_I/r_O = 0.48$. In the present work, $\bar{P}^*$ is reported in the SI units of kg·m/[s·m²·(N/m²)], where the pressure is expressed in Pascals (N/m²). Since $1N = 1$ kg m/s², the units of $\bar{P}^*$ are just seconds (s). These units do not appear to have been used heretofore. Permeability coefficients have often been reported in the literature in units of cubic centimeters (STP) cm/(s·cm²·cm Hg), and these should be multiplied by $3.3464 \times 10^{-9}\ M$, where $M$ is the molecular weight of the gas, to obtain SI units. The maximum error in $\bar{P}^*$ has been estimated to be ±7%.

The permeability coefficients are exponential functions of the temperature at constant $\Delta p$ (Stern, 1972*b*):

$$\bar{P} = A \exp(-E_p/RT) \qquad (8)$$

The dependence of $\bar{P}$ on temperature is illustrated in Figure 10 by Arrhenius plots for the three gases studied.

Table 3. Comparison of Gas Permeability Measurements in Silicone Rubber Membranes

| Reference | Temp., $t$(°C) | Permeability coefficient, $\bar{P}^* \times 10^{16}$(s)† $N_2$ | $O_2$ | Ar | Filler content | Remarks |
|---|---|---|---|---|---|---|
| Barrer and Chio | 0 | 22.5 | 55.5 | 77.8 | 9.1 wt % Santocel CS (dens.: $1.66 \times 10^3$ kg/m³); vol. fr.: 0.0554 | Plane sheet, $2.06 \times 10^{-3}$ m-thick (Imperial Chemical Ind., U.K.) |
| Barrer and Chio | 0 | 19.1 (−0.8°C) | 50.4 | 69.8 | 32.8 wt % Aerosil K3 silica (dens.: $2.20 \times 10^3$ kg/m³); vol. fr.: 0.182 | Tubing, $1.15 \times 10^{-2}$ m O.D. × $7.01 \times 10^{-3}$ m I.D. (Midland Silicones, U.K.) |
| This work†† | 0 | 18.6 | 50.0 | 63.6 | 51.7 wt % silica (dens.: $2.20 \times 10^3$ kg/m³); vol. fr.: 0.3225 | Hollow fibers, $6.35 \times 10^{-4}$ m O.D. × $3.05 \times 10^{-4}$ m I.D. (Silastic Medical Grade—Dow-Corning Co.) |
| Robb | 25 | 31.9 | 78.2 | 97.6 | 33 wt % silica (assumed dens.: $2.20 \times 10^3$ kg/m³); vol. fr.: 0.182 | Plane sheet (General Electric Co.) |
| This work† | 25 | 29.0 | 70.7 | 90.0 | 51.7 wt % silica (dens.: $2.20 \times 10^3$ kg/m³); vol. fr.: 0.3225 | Hollow fibers, $6.35 \times 10^{-4}$ m O.D. × $3.05 \times 10^{-4}$ m I.D. (Silastic Medical Grade—Dow-Corning Co.) |

† Permeability coefficients were corrected for filler content by dividing $\bar{P}$ by the volume fraction of filler.
†† For unstresseed fibers.

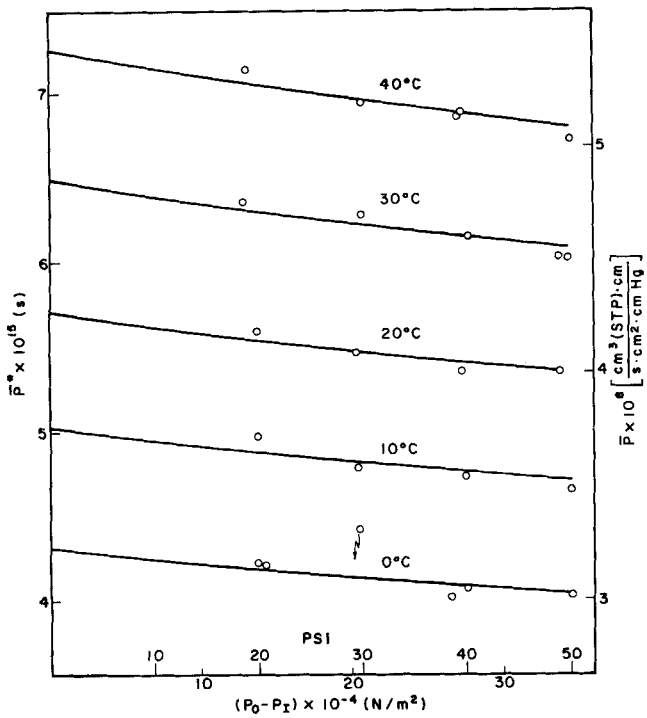


**Fig. 9. Effective permeability coefficient for argon as a function of pressure difference across fiber wall.**

The origin of this figure is described later.

The permeability coefficients obtained in this work are compared in Table 3 with the results of Barrer and Chio (1965) at 0°C and of Robb (1965) at 25°C. The values of $\bar{P}$ were corrected for filler volume. Barrer and Chio, as well as Robb, obtained their data at low pressures. The values of the present work were accordingly calculated from the equations of Figure 10 for unstressed fibers. Table 3 shows that $\bar{P}$ decreases with increasing filler content. This may be the result of the filler particles acting as cross-linking agents and producing a tighter chain network (Barrer and Chio, 1965). Table 4 compares the energies of activation for the permeation process calculated from Equation (8) with pertinent literature data. The agreement is as good as can be expected for such data, considering the differences in filler content, distribution, and particle size and shape. The low energies of activation have been attributed to the ease of segmental motion about the silicon-oxygen linkage.

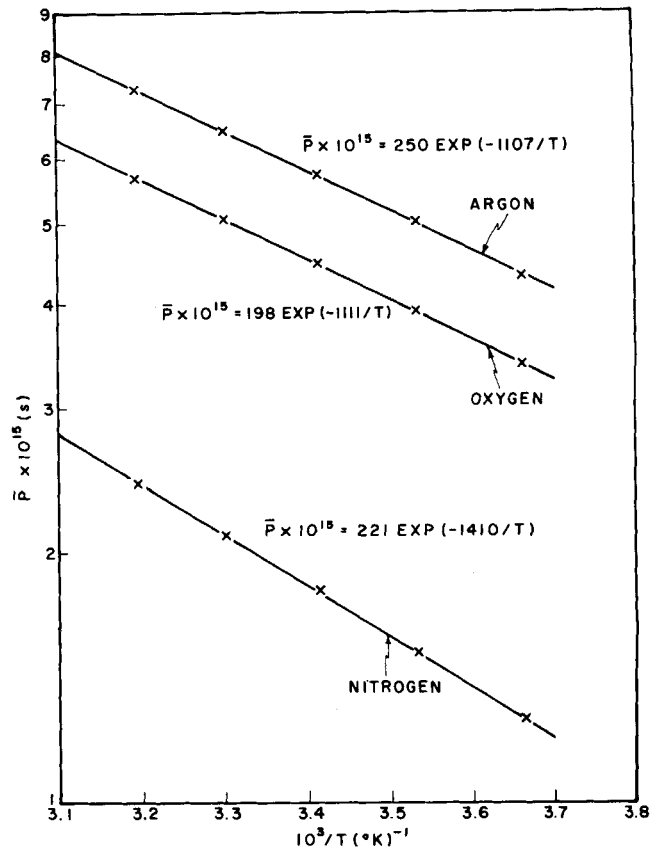


**Fig. 10. Dependence of permeability coefficients for nitrogen, oxygen, and argon on temperature. The permeability coefficients are for unstressed fibers.**

It is interesting to note from Figures 7, 8, and 9 that $\bar{P}^*$ decreases with increasing $\Delta p$ at constant temperature. This behavior is due, in negligible part, to a decrease in the free volume of the penetrant gas + polymer system, which is predicted by a free-volume model of gas permeation (Stern et al., 1972*a*). Most of the decrease in $\bar{P}^*$ is due to the elastic deformation of the follow fibers.

### Permeation of Gas Mixtures

The performance of the permeator was investigated by studying the permeation behavior of synthetic air at 10°C and $\Delta p$'s of $2.07 \times 10^5$ and $3.45 \times 10^5$ N/m² (30 and 50 lb/in.²). In both cases, $p_I$ was near $1 \times 10^5$ N/m² (14.7 lb/in.² abs). The experimental results are

Table 4. Comparison of Energies of Activation for Gas Permeation in Silicone Rubber Membranes

| Reference | Temperature range, $\Delta t$ (°C) | Energy of activation, $E_p$ (kcal/k mole) $N_2$ | $O_2$ | Ar | Remarks |
|---|---|---|---|---|---|
| Barrer and Chio | 0 to −37 | 2 600 | 2 070 | 2 320 | Plane sheet, $2.06 \times 10^{-3}$ m-thick (Imperial Chemical Ind.) |
| Barrer and Chio | 0 to −40 | 3 280 | 2 590 | 2 540 | Tubing, $11.5 \times 10^{-3}$ m O.D. × $7.0 \times 10^{-3}$ m I.D. (Midland Silicones) |
| Reitlinger et al. | 21 to 111 | 2 700 | 1 725 | — | Plane sheet, $1.0 \times 10^{-3}$ m-thick (prepared by authors) |
| This work* | 0 to 50 | 2 800 | 2 210 | 2 200 | Hollow fibers, $6.35 \times 10^{-4}$ m O.D. × $3.05 \times 10^{-4}$ m I.D. (Silastic Medical Grade—Dow Corning Co.) |

* Average values for Δp between 0 and $3.45 \times 10^5$ N/m² (50 psi) for unstressed fibers.

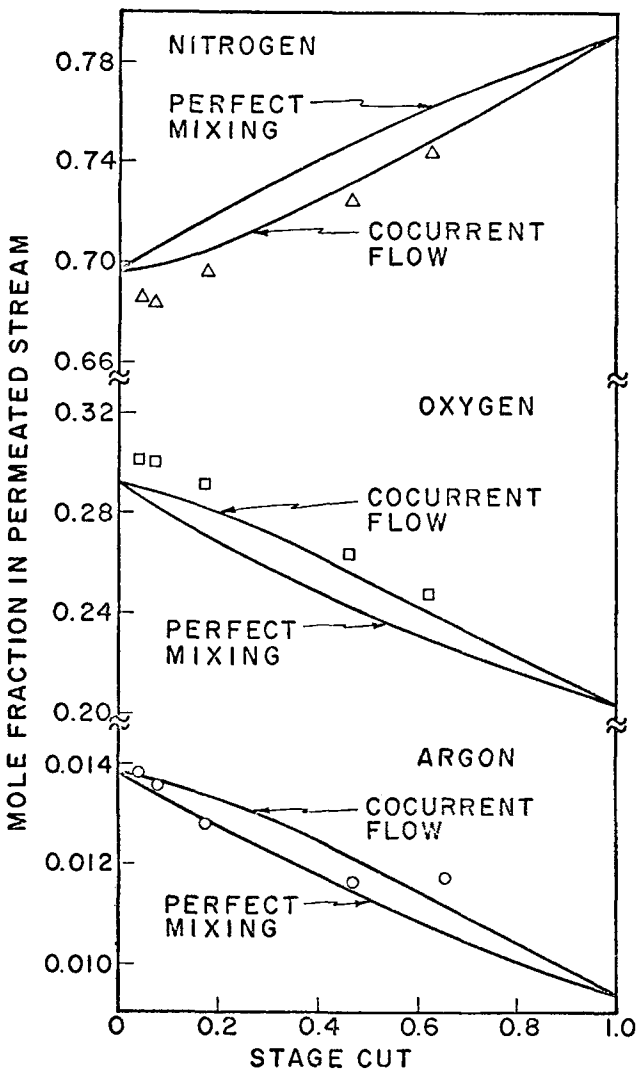


Fig. 11. Separation of air by selective permeation at 10.0°C and $\Delta p = 2.07 \times 10^5$ N/m² (30 lb/in.²). Composition of permeated stream as a function of stage cut. Theoretical results are indicated by solid lines.

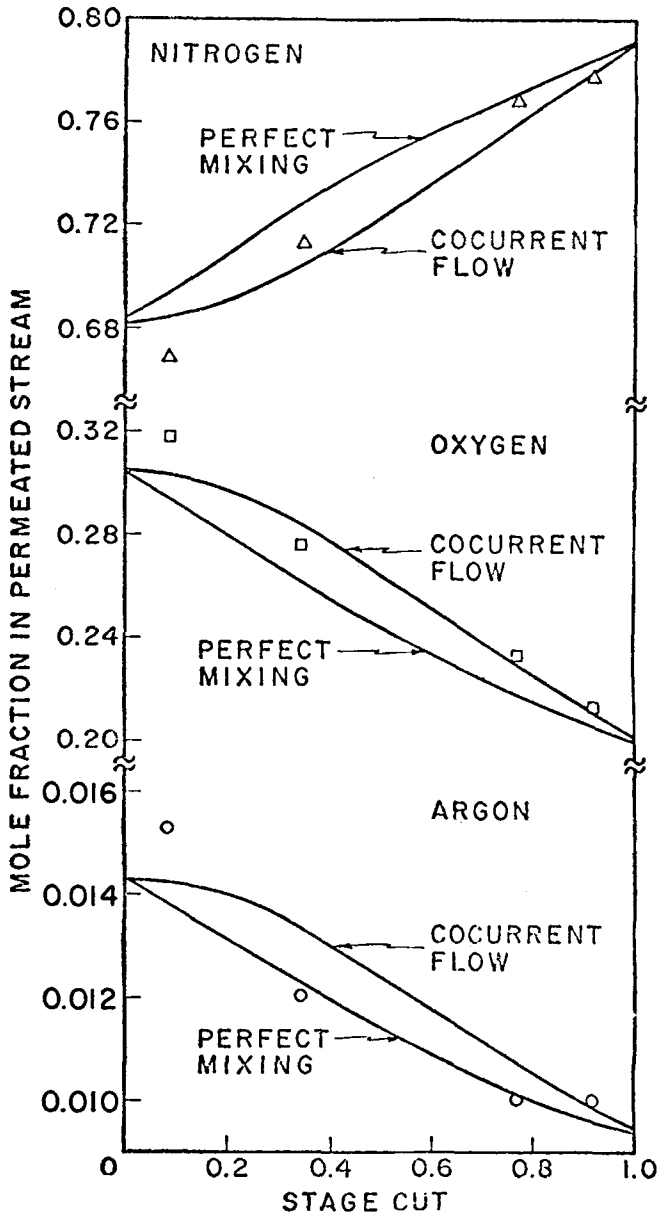


Fig. 12. Separation of air by selective permeation at 10.0°C and $\Delta p = 3.45 \times 10^5$ N/m² (50 lb/in.²). Composition of permeated stream as a function of stage cut. Theoretical results are indicated by solid lines.

presented graphically in Figures 11 and 12, where the composition of the permeated (low pressure) streams is shown as a function of the stage cut, that is, the fraction of the feed permeating through the fibers.

The permeated and unpermeated streams were allowed to flow cocurrently to one another. The gas-chromatographic analysis of the gas streams was made with a column of Molecular Sieve 5A at the temperature of dry ice. The accuracy of the measurements was generally within the accepted limits for this type of analysis (Krugers, 1968):

| Concentration, in vol % | Standard deviation, in % |
|---|---|
| 0.05 – 0.5 | > 50 |
| 0.5 – 3 | 5-10 |
| 3 – 10 | 3-5 |
| > 30 | < 2 |

It is seen from Figures 11 and 12 that the permeated stream was enriched in oxygen and argon by comparison with the feed stream, particularly at $3.45 \times 10^5$ N/m² (50 lb/in.²), and that this enrichment increased markedly at low stage cuts. It is unlikely, however, that stage cuts much smaller than about 0.3 will be used in practice. The separation of oxygen and argon from air by selective permeation through silicone rubber is a difficult process because the ideal separation factors for oxygen-nitrogen and argon-nitrogen are small.

## COMPARISON OF THEORY WITH EXPERIMENT

### Permeability Coefficients for Pure Gases

Comparison of Equations (2) and (7) shows that

$$\overline{P}^* = \overline{P} f_1 \tag{9}$$

and this equation was used to plot the theoretical curves in Figures 7, 8, and 9. In order to obtain the theoretical curve associated with a particular gas at a particular temperature, it was necessary to use the data in Table 1 and to know the permeability coefficient $\overline{P}$ and Young's modulus $E$. Direct measurements of $E$ in the transverse and axial directions of the fibers yielded the values of $4.53 \times 10^6$ N/m² (657 lb/in.²) and $1.66 \times 10^6$ N/m² (240 lb/in.²) respectively. Blaisdell and Kammermeyer (1972) have reported similar values for fine-bore silicone rubber tubing, namely,

$4.14 \times 10^6$ to $4.82 \times 10^6$ N/m$^2$ (600 to 700 lb/in.$^2$) in the radial direction and $2.07 \times 10^6$ (300 lb/in.$^2$) in the axial direction. Since the elastic deformation analysis employed in this study is applicable only to isotropic materials, an average value of $3.09 \times 10^6$ N/m$^2$ (448 lb/in.$^2$) was taken for $E$, based on the present measurements. Any possible dependence of $E$ on temperature was neglected. The permeability coefficient $\overline{P}$ was regarded as an adjustable constant to be selected on the basis of the best overall fit to the test data in a least-squares sense. The best values of $\overline{P}$ arrived at can be read from the intercepts of the solid curves with the vertical axes in Figures 7, 8, and 9, since $f_1 = 1$ at $p_O - p_I = 0$ and thus $\overline{P}^* = \overline{P}$.

The agreement between theory and experiment in Figures 7, 8, and 9 can be considered promising. Despite some scatter, the experimental data clearly suggest a certain concavity in the relationship between $\overline{P}^*$ and $p_O - p_I$, and the same type of concavity is exhibited by the theoretical curve. An analysis based on infinitesimal elasticity would have led to the wrong kind of concavity, as is demonstrated by the dashed curve labeled linear elasticity in Figure 7.

It should be noted that because of the relatively small range of pressures covered in the permeation measurements, the curve fitting is not too sensitive to $E$. That is to say, overall agreement between theory and experiment almost as good as that shown in Figure 7, 8, and 9 can be obtained with values of $E$ that deviate considerably from the value of $3.09 \times 10^6$ N/m$^2$ (448 lb/in.$^2$). In general, an increase in the selected value of $E$ tends to straighten the theoretical curves and lower their intercepts (see argon at 40°C), while a reduction in $E$ has the opposite effects.

#### Arrhenius Plots of Permeability Coefficients

The intercepts of the solid curves in Figures 7, 8, and 9 with the vertical axes represent combined theoretical-experimental estimates of the permeability coefficients $\overline{P}$. These intercepts are used as the basis of the Arrhenius plots in Figure 10, showing the dependence of $\overline{P}$ on temperature for each of the three gases used in the experiments. From these plots, one can obtain the equations shown on the figure for the dependence of $\overline{P}$ on the temperature.

#### The Separation of Air

The separation of air in the hollow fiber permeator was predicted for the experimental conditions on the basis of the following two theoretical models:

1. Cocurrent flow of the gas streams inside and outside the hollow fibers, as was the case in the experimental work, but assuming that no mixing occurred in either stream.

2. Perfect mixing in the two gas streams. These models have been discussed in the literature in some detail (Hwang and Kammermeyer, 1975; Stern, 1972*b*; Walawender and Stern, 1972; Stern and Walawender, 1969). It is assumed that the permeability coefficients for the individual components of a gas mixture are the same as for the pure components. This implies that the components of the permeating mixture do not interact with each other; such a behavior can be expected for gases with low critical temperatures, such as oxygen, nitrogen, and argon, which exhibit a very low solubility in polymers. Therefore, the values of $\overline{P}^*$ used are those given in Figures 7, 8, and 9 at the appropriate pressures and temperature.

The theoretical results are compared with the experimental data in Figures 11 and 12. The latter appear to be either close to the compositions predicted for cocurrent flow, as would be expected, or to lie in-between those for cocurrent flow and perfect mixing. The difference between these two flow patterns is relatively small for small separation factors (Stern and Walawender, 1969). The agreement must be considered as satisfactory, allowing for the magnitude of the experimental error and the assumptions made in the calculations. It has been mentioned previously that Blaisdell and Kammermeyer (1973) and Thorman, Rhim, and Hwang (1975) have also reported agreement between theory and experiment for the permeation of oxygen-nitrogen mixtures at lower pressures. Consequently, the separation of mixtures of simple gases by means of hollow silicone rubber fibers can be predicted with some confidence from idealized theoretical models, at least at gauge pressures up to $3.45 \times 10^5$ N/m$^2$ (50 lb/in.$^2$ gauge).

Calculations show that two potentially useful products are obtained when air is separated in a single permeation stage using silicone rubber membranes. At $\Delta p \geq 3.45 \times 10^5$ N/m$^2$ (50 lb/in.$^2$) and a stage cut of 0.4, the permeated stream contains at least 28 mole % oxygen. This oxygen enriched air may find a variety of biomedical and industrial applications. On the other hand, the unpermeated stream obtained at a stage cut of 0.8 contains about 9 mole % oxygen. Such an oxygen-depleted gas stream may find applications for the inerting of fuel tanks of jet transports.

## REMARKS ON THE CONSTRUCTION OF PERMEATORS

The present study provides new information on the design of permeators using hollow silicone rubber fibers as separation barriers. When pressurized externally, single hollow fibers undergo two types of elastic deformation: the cross-section decreases, causing an increase in the ratio $R_O/R_I$, and the length of the fiber increases, thus providing more permeation area. The former effect causes a decrease in the rate of gas permeation, while the latter increases the permeation rate. Figure 1 shows that for isotropic fibers with $n > 0.25$, the increase in the $R_O/R_I$ ratio is more important at lower pressures, whereas the fiber elongation is predominant at higher pressures. As a result, the correction factor $f_1$ passes through a minimum as the dimensionless pressure difference across the fiber wall $(p_O - p_I)/E$ is increased. In the case of thick walled fibers, for which $n \leq 0.25$, the increase in fiber length is the main effect at all pressures.

In the permeator shown in Figure 5, the hollow fibers were deliberately separated from each other because it was desired to study gas permeation through isolated fibers. However, a practical permeator for a large scale permeation process will be fully packed with fibers in order to maximize the ratio of permeation area-to-permeator volume and thus minimize the capital investment costs. Of course, some spacing must be maintained between the fibers in order to prevent an excessive pressure drop in, and uneven distribution of, the high-pressure gas stream. It is conceivable that such a spacing could be provided by some powder of suitable particle size. The permeability and elastic behavior of the fibers will depend on the operating conditions of the permeator. If the value of $(p_O - p_I)/E$ is such that the correction factor $f_1$ is less than unity, the rate of gas permeation will be smaller than that obtained with unstressed fibers. This effect is undesirable. The decrease in the fiber cross-

section will lower somewhat the pressure drop in the high-pressure gas stream, but this is probably not an important benefit. On the other hand, if $(p_O - p_I)/E$ is sufficiently large so that $f_1$ is greater than unity, the permeation rate will be larger than found with unstressed fibers for the reasons mentioned above. This is a desirable effect.

The elongation of the hollow fibers due to external pressure may possibly result in an additional effect. Since the fiber packing density in a practical permeator will be high and the fiber ends will most likely be encased in fixed headers, the elongated fibers will compete for space and probably press against each other as the pressure is raised. The resulting fiber distortion may increase the pressure drop in the high- and low-pressure gas streams, that is, in the streams outside and inside the hollow fibers, respectively. One may then expect a decrease in permeation rate. The separation efficiency will also be adversely affected owing to mixing in the gas streams induced by the distorted flow paths.

The importance of this effect will depend on the Poisson type of coupling between axial elongation and radial pressure. The smaller this coupling, the smaller also the percent elongation of the fibers. In the present study it was assumed, in order to simplify the analysis, that the fibers are isotropic incompressible materials, and this leads to a rather significant Poisson effect. However, the fibers are in fact anisotropic, as evidenced by the markedly different measured values of $E$ for the axial and transverse directions. Consequently, it is quite possible for the Poisson effect to be less important than would appear from Table 1 or Figures 1 and 2, and this has been borne out by some preliminary direct observations of fiber slackening under external pressure. Further experimental work and theoretical refinement are needed in order to obtain a model of fiber behavior that properly reflects the axial extensions resulting from external pressure.

It is interesting to consider the use as separation barriers of (yet hypothetical) hollow elastic fibers which would increase markedly in length under external pressure. A simple solution then suggests itself to the above problems, namely, that the unpressurized fibers be mounted in the permeator under tension. The application of external pressure will then tend to relax the tension rather than increase the length of the fibers. The initial tension can be adjusted so that it is completely relaxed only when the operating pressure is attained. The use of fibers under tension will also permit a higher packing density because of the reduction of the fiber cross section. The required tension can be determined from an extension of the analysis presented in the Appendix to anisotropic elastic fibers.


## ACKNOWLEDGMENT

The financial assistance of the Energy Research and Development Administration under Grant No. AT(11-1)3536 is gratefully acknowledged. The authors also wish to thank Mr. S.-C. Wang for assisting with computations.


## NOTATION

$A$ = constant in Equation (8)
$E$ = Young's modulus
$E_p$ = energy of activation for permeation process
$e_a$ = engineering principal strain in axial direction
$e_c$ = engineering principal strain in circumferential direction
$e_r$ = engineering principal strain in radial direction
$f_1$ = function defined by Equation (3)
$f_2$ = function defined by Equation (5)
$G$ = rate of gas permeation
$L$ = length of stressed fiber exposed to gas
$l$ = length of unstressed fiber exposed to gas
$n$ = ratio of internal-to-external radii of unstressed fiber, $r_I/r_O$
$\overline{P}$ = permeability coefficient for unstressed fibers ($\Delta p = 0$)
$\overline{P}^*$ = effective permeability coefficient, $\overline{P}f_1$
$p_O, p$ = gas pressure outside hollow fiber
$p_I$ = gas pressure inside hollow fiber
$Q$ = contraction ratio of outer radius, $R_O/r_O$
$q$ = contraction ratio of inner radius, $R_I/r_I$
$R$ = universal gas constant
$R_I$ = inner radius of stressed fiber
$R_O$ = outer radius of stressed fiber
$r_I$ = inner radius of unstressed fiber
$r_O$ = outer radius of unstressed fiber
$r$ = initial radial coordinate of a material point
$r'$ = current radial coordinate of a material point, $r + u_r$
$T$ = absolute temperature
$t_a$ = principal normal stress in axial direction
$t_c$ = principal normal stress in circumferential direction
$t_r$ = principal normal stress in radial direction
$t_h$ = hydrostatic tension
$u_r$ = radial displacement (positive outward) of a material point
$\Delta p$ = pressure drop across fiber wall, $p_O - p_I$
$\epsilon$ = parameter defined by Equation (A11)

## LITERATURE CITED


Barrer, R. M., and H. T. Chio, *J. Polymer Sci, C10*, 111 (1965).

Blaisdell, C. T., and K., Kammermeyer, *AIChE J.*, **18**, 1015 (1972).

———, *Chem. Eng. Sci.*, **28**, 1249 (1973).

Hwang, S.-T., and K. Kammermeyer, *Membranes in Separations*, Wiley-Interscience, New York (1975).

Krugers, J., ed., *Instrumentation in Gas Chromatography*, Centrex Publishing Co., Eindhoven (1968).

Mattson, R. J., and V. J. Tomsic, *Chem. Eng. Progr.*, **65**, 62 (1969).

McAfee, K. B., *Encyclopedia of Chemical Technology*, A. Stauden, ed., 2 supplement, pp. 297-315, Interscience, New York (1960).

Reitlinger, S. A., A. A. Maslennikova, and I. S. Iarkho, *Soviet Phys. Tech. Phys.*, **1**, 2467 (1956).

Robb, W. L., "Thin Silicone Membranes—Their Permeation Properties and Some Applications," Rep. No. 65-C-031, Research and Development Center, General Electric Co., Schenectady, N. Y. (Oct., 1965).

Stern, S. A., and W. P. Walawender, *Separation Sci.*, **4**, 129 (1969).

Stern, S. A., S.-M. Fang, and H. L. Frisch, *J. Polymer Sci.*, A-2, **10**, 201 (1972*a*).

Stern, S. A., *Industrial Processing with Membranes*, R. E. Lacev and S. Loeb, ed., Chapt. XIII, pp. 279-339, Wiley-Interscience, New York (1972*b*).

Thorman, J. M., H. Rhim, and S.-T. Hwang, *Chem. Eng. Sci.*, **30**, 751 (1975).

Varga, O. H., *Stress-Strain Behavior of Elastic Materials*, Interscience, New York (1966).

Walawender, W. P., and S. A. Stern, *Separation Sci.*, **7**, 553 (1972).

Yasuda, H., V. Stannett, H. L. Frisch, and A. Peterlin, *Makromol. Chem.*, **73**, 188 (1964).


## APPENDIX: DEFORMATION ANALYSIS OF ELASTIC TUBES UNDER EXTERNAL PRESSURE

Varga (1966) has presented a large deflection analysis of thick walled isotropic incompressible elastic tubes under internal pressure, based on a rather simple stress-strain law.

Here we modify Varga's analysis slightly to arrive at equations defining the deformations of such tubes when the pressure is external rather than internal.

We take as the datum state the tube under $1 \times 10^5$ N/m$^2$ (14.7 lb/in.$^2$ abs) of hydrostatic pressure. That is to say, the strains and stresses of the tube in that state are defined as zero. Consequently, in the following development the external pressure $p$ and the internal pressure of zero will be understood to be gauge pressures. Similarly, any normal stresses in the material will be understood to be not total stresses but stresses that are superimposed on the initial hydrostatic compressive stress of 1 atm.

Varga's stress-strain relations [(V.1.5 of Varga (1966)] involve a single material constant, the Young's modulus $E$, which is defined as the initial slope of the stress-strain curve obtained in a conventional uniaxial tension test at standard atmospheric pressure. The stress-strain relations themselves are

$$t_c = \frac{2}{3}Ee_c + t_h$$

$$t_r = \frac{2}{3}Ee_r + t_h \qquad \text{(A1)}$$

$$t_a = \frac{2}{3}Ee_a + t_h$$

where $t_c$, $t_r$, $t_a$ are the principal normal stresses (positive for tension) in the circumferential, radial, and axial directions, respectively; $e_c$, $e_r$, $e_a$ are the corresponding engineering principal strains, and $t_h$ is the elastically indeterminate hydrostatic tension required in the stress-strain relations for isotropic incompressible materials.

The following notation will be needed in addition to that which has already been introduced:

$q$ = $R_I/r_I$ = contraction ratio of inner radius
$Q$ = $R_O/r_O$ = contraction ratio of outer radius
$r$ = initial radial coordinate of a material point
$u_r$ = radial displacement (positive outward) of a material point
$r'$ = $r + u_r$ = current radial coordinate of a material point

With the above preliminaries out of the way, we now turn to the analysis proper. We start by noting that Varga's derivation for internal pressure [(Chapter V. of Varga (1966)] up and including his Equation (V.1.7.) applies equally well to the case of external pressure. From it we have the following expressions for $e_r$ and $t_h$:

$$e_r = \frac{(Q^2 - n^2q^2)^{1/2}}{1 - n^2}\left[1 - n^2 - \frac{q^2 - Q^2}{(r'/r_I)^2}\right]^{1/2} - 1 \qquad \text{(A2)}$$

$$t_h = \frac{2}{3}E\left(1 - \frac{1 - n^2}{Q^2 - n^2q^2}\right) \qquad \text{(A3)}$$

Substituting (A3) and (A2) into the second of Equations (A1) and setting $r'$ equal to $R_I$, we obtain the following expression for the normal stress on the inner surface of the tube:

$$(t_r)_{r'=R_I} = \frac{2}{3}E\left[\frac{Q^2 - n^2q^2}{(1 - n^2)q} - \frac{1 - n^2}{Q^2 - n^2q^2}\right] \qquad \text{(A4)}$$

Since the pressure is atmospheric on the inside of the tube, the above stress must vanish, which leads to the following relationship between $q$ and $Q$:

$$Q = \sqrt{n^2q^2 + (1 - n^2)}\sqrt{q} \qquad \text{(A5)}$$

Again substituting (A3) and (A2) into the second of Equations (A1), but this time setting $r'$ equal to $R_O$, we obtain

$$(t_r)_{r'=R_O} = \frac{2}{3}E\left(\frac{1 - n^2}{Q^2 - n^2q^2}\right)\left(\frac{q}{Q} - 1\right) \qquad \text{(A6)}$$

as the normal stress on the outer surface. The left side of this equation may be replaced by $-p$, where $p$ is the external gauge pressure, and on the right side $Q^2 - n^2q^2$ may be replaced by $(1 - n^2)\sqrt{q}$, in accordance with Equation (A5). Thus, the following formula is obtained for $p$:

$$p = \frac{2}{3}E\frac{1}{\sqrt{q}}\left(1 - \frac{q}{Q}\right) \qquad \text{(A7)}$$

Implicit in the above analysis is the assumption that the axial elongation accompanying the radial contraction is free to take place without restraint. The strain $e_a$ associated with this elongation is given by Varga's Equation (V.1.3.c) as

$$e_a = \frac{1 - n^2}{Q^2 - n^2q^2} - 1$$

With $Q^2 - n^2q^2$ once again replaced by $(1 - n^2)\sqrt{q}$, this becomes

$$e_a = \frac{1}{\sqrt{q}} - 1 \qquad \text{(A8)}$$

Equations (A5), (A7), and (A8) are the essential results of the present analysis. In using them it is best to regard $q$ as the independent variable, choosing values which start at 1 and diminish toward zero. For any value of $q$, the corresponding values of $Q$ and $e_a$ can be obtained from Equations (A5) and (A8), and the external pressure $p$ needed to maintain the given $q$ can be found from Equation (A7).

Recognizing that $L/l = 1 + e_a$, $r_O/r_I = 1/n$, and $R_O/R_I = Q/nq$, we can convert Equation (3) to

$$f_1 = (1 + e_a)\frac{\ln(n)}{\ln(nq/Q)} \qquad \text{(A9)}$$

and this equation can be used to find the value of $f_1$ associated with any given $q$ once the corresponding $Q$ and $e_a$ have been determined from Equations (A5) and (A8). The pressure for which this $f_1$ value applies is that given by Equation (A7). Figure 1 and Table 1 were obtained in the manner just described, using the notation $p_O - p_I$ in place of $p$.

The deformations associated with infinitesimal elasticity theory can be derived by setting $q = 1 - \epsilon$ in Equations (A5), (A7), and (A8), expanding in powers of $\epsilon$, and retaining terms up to the first degree in $\epsilon$. This procedure leads to

$$p = \epsilon \cdot E(1 - n^2)/2$$

$$Q = 1 - [\epsilon \cdot (1 + 3n^2)/4] \qquad \text{(A10)}$$

$$e_a = \epsilon/2$$

From the first of these equations it follows that

$$\epsilon = \frac{2(p/E)}{1 - n^2} \qquad \text{(A11)}$$

and therefore

$$q = 1 - \frac{2(p/E)}{1 - n^2}$$

$$Q = 1 - \frac{(p/E)(1 + 3n^2)}{2(1 - n^2)} \qquad \text{(A12)}$$

$$e_a = \frac{(p/E)}{1 - n^2}$$

Equations (A12) agree exactly with the classical Lamé solution when Poisson's ratio in that solution is set equal to 0.5, the value associated with incompressible materials. The substitution of expressions (A12) in Equation (A9) leads to the dashed curves in Figures 1 and 7.

*Manuscript received August 2, 1976; revision received May 9 and accepted May 12, 1977.*